

Experimental verification of five-qubit quantum error correction with superconducting qubits

Ming Gong,^{1,2} Xiao Yuan,^{1,2,3,4} Shiyu Wang,^{1,2} Yulin Wu,^{1,2} Youwei Zhao,^{1,2} Chen Zha,^{1,2} Shaowei Li,^{1,2} Zhen Zhang,³ Qi Zhao,³ Yunchao Liu,³ Futian Liang,^{1,2} Jin Lin,^{1,2} Yu Xu,^{1,2} Hui Deng,^{1,2} Hao Rong,^{1,2} He Lu,^{1,2} Simon C. Benjamin,⁴ Cheng-Zhi Peng,^{1,2} Xiongfeng Ma,³ Yu-Ao Chen,^{1,2} Xiaobo Zhu,^{1,2} and Jian-Wei Pan.^{1,2}

¹ Hefei National Laboratory for Physical Sciences at Microscale and Department of Modern Physics, University of Science and Technology of China, Hefei, Anhui 230026, China

² Shanghai Branch, CAS Center for Excellence and Synergetic

Innovation Center in Quantum Information and Quantum Physics, University of Science and Technology of China, Shanghai 201315, China

³ Center for Quantum Information, Institute for Interdisciplinary Information Sciences, Tsinghua University, Beijing 100084, China and

⁴ Department of Materials, University of Oxford, Parks Road, Oxford OX1 3PH, United Kingdom

(Dated: June 27, 2022)

Quantum error correction is an essential ingredient for universal quantum computing [1–5]. Despite tremendous experimental efforts in the study of quantum error correction [6–8], to date, there has been no demonstration in the realisation of universal quantum error correction code (QECC), with the subsequent verification of all key features including the identification of an arbitrary physical error, the capability for transversal manipulation of the logical state, and state decoding. To address this notoriously difficult challenge, we push the limits of the depth of superconducting quantum circuits and experimentally realise the universal five-qubit QECC [4, 5], the so-called smallest perfect code that permits corrections of generic single-qubit errors. In the experiment, having optimised the encoding circuit, we employ an array of superconducting qubits to realise the five-qubit QECC for several typical logical states including the magic state, an indispensable resource for realising non-Clifford gates. The encoded states are prepared with an average fidelity of 57.1(3)% while with a high fidelity of 98.6(1)% in the code space[7]. Then, the arbitrary single-qubit errors introduced manually are identified by measuring the stabilizers. We further implement logical Pauli operations with a fidelity of 97.2(2)% within the code space. Finally, we realise the decoding circuit and recover the input state with a process fidelity of 57.4(7)%. After decoding, by identifying errors via the measurement of the four ancillae and then mathematically recovering the qubit state, we verify the power of error correction of this code. Thus, by demonstrating each key aspect of error correction with the five-qubit code, our work establishes the viability of experimental quantum error correction with superconducting qubits and paves the route

to fault-tolerant quantum computing.

Quantum computers can tackle classically intractable problems [9] and efficiently simulate many-body quantum systems [10]. However, quantum computers are notoriously difficult to control, due to their ubiquitous yet inevitable interaction with their environment, together with imperfect manipulations that constitute the algorithm. The theory of QECCs and fault tolerance has been developed as the long-term solution to this issue, enabling universal error-free quantum computing with noisy quantum hardware [1]. The logical qubits of an algorithm can be represented using a larger number of flawed physical qubits. Providing that the machine is sufficiently large (high qubit count), and that physical errors happen with a probability below a certain threshold, then such errors can be systematically detected and corrected [11, 12]. In experiment, there have been successful efforts of realizing small QECCs with optics [13–15], ion traps [7, 16–18], superconducting qubits [6, 19–21], and others [8, 22, 23]. However, due to the limitation of inaccurate operations on a restricted number of qubits, previous experiments only implement codes for correcting certain types of errors or preparing certain logical states. It remains an open challenge to realise a fully-functional QECC.

To address the challenge, we focus on the five-qubit code, the ‘perfect’ code that can protect a logical qubit from an arbitrary single physical error using the smallest number of qubits [4, 5]. It is a type of stabilizer code that is defined by a set of independent operators from the Pauli group, called stabilizers, such that the code space only has eigenvalue +1. The four stabilizers of the five-qubit code are

$$\begin{aligned} g_1 &= X_1 Z_2 Z_3 X_4 I_5, \quad g_2 = I_1 X_2 Z_3 Z_4 X_5, \\ g_3 &= X_1 I_2 X_3 Z_4 Z_5, \quad g_4 = Z_1 X_2 I_3 X_4 Z_5, \end{aligned} \quad (1)$$

with I_i , X_i , Y_i , Z_i being the Pauli matrices acting on the i^{th} qubit. The logical state space is defined by states

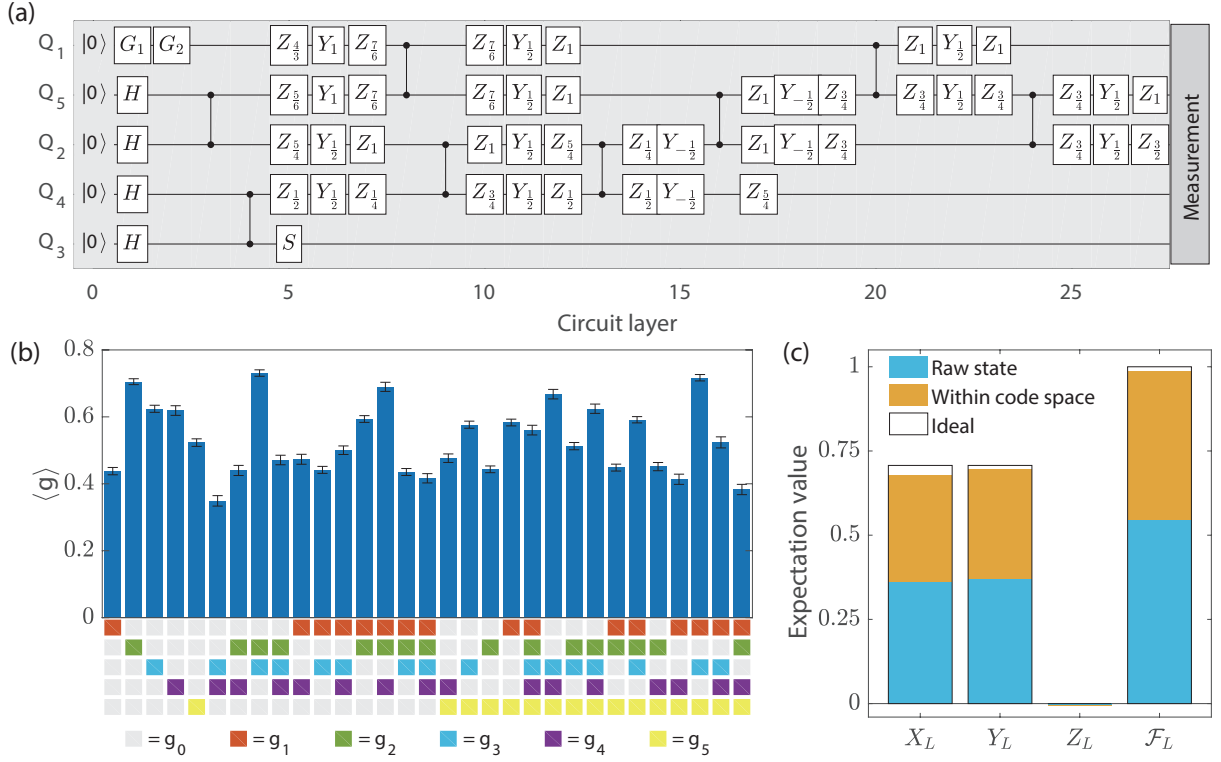


FIG. 1. (a) Encoding quantum circuit of the five-qubit code. Here, the qubit label $Q_1 \sim Q_5$ is arranged to correspond with Eq. (1). G_1 and G_2 are single-qubit gates to prepare the input state $a|0\rangle + b|1\rangle$ for encoding. Y_α and Z_α are the rotation gates around Y - and Z -axis for an angle $\alpha\pi$, respectively. In total, there are 27 layers of gate operations, including 54 single-qubit gates, and 8 nearest-neighbour controlled-phase gates. The single-qubit gates on different qubits can be applied in parallel, while the two-qubit gates can only be applied individually owing to the Z -crosstalk. (b) Expectation values of 31 stabilizers for the encoded logical state $|T\rangle_L$. We apply quantum state tomography to obtain the density matrix ρ_q of the prepared logical states. Any logical state $|\Psi\rangle_L = a|0\rangle_L + b|1\rangle_L$ can be uniquely determined by the four stabilizers defined in Eq. (1) together with the fifth stabilizer $g_5 = |\Psi\rangle_L \langle\Psi|_L - |\Psi^\perp\rangle_L \langle\Psi^\perp|_L = (aa^* - bb^*)Z_L + (a^*b + b^*a)X_L - i(a^*b - b^*a)Y_L$, with $|\Psi^\perp\rangle = b^*|0\rangle_L - a^*|1\rangle_L$. That is, any logical state $|\Psi\rangle_L$ can be decomposed as $|\Psi\rangle_L \langle\Psi|_L = 2^{-5} \Pi_{i=1}^5 (g_0 + g_i)$, where $g_0 = I_1 I_2 I_3 I_4 I_5$ is the trivial stabilizer of all pure quantum states. Therefore the fidelity between the experimentally prepared state and the ideal state $|\Psi\rangle_L \langle\Psi|_L$ can be also determined by the measurement of the 32 stabilizer operators in $\Pi_{i=1}^5 (g_0 + g_i)$. We omit the g_0 one as it is constantly 1. In this way, we obtained the state fidelity as the average of the 32 stabilizers by picking up corresponding measurement results among the tomography results. Finally, the state fidelity of $|T\rangle_L$ reaches 54.5(4)%. Error bars representing a 95% confidence interval are estimated via bootstrapping. (c) Expectation values of logical Pauli operators and state fidelity of the encoded magic state $|T\rangle_L$. The state fidelity is improved from 54.5(4)% to 99.3(1)% by projecting the state in the code space. The probability that the state is in the code space is 53.2(4)%.

$|\Psi\rangle_L = a|0\rangle_L + b|1\rangle_L$ that are simultaneously stabilized by the four stabilizers with $g_i |\Psi\rangle_L = +|\Psi\rangle_L, \forall i = 1, 2, 3, 4$. Here the logical states $|0\rangle_L$ and $|1\rangle_L$ are the basis states that are eigenstates of the logical Z_L operator and logical Pauli operators can be transversally realised by applying the corresponding single-qubit gates on each physical qubit, $\sigma_L = \sigma_1 \sigma_2 \sigma_3 \sigma_4 \sigma_5$ for $\sigma = X, Y, Z$. General logical operators, such as the $T_L = e^{-iZ_L \pi/8}$ gate, may not be transversally realised. In experiment, we realise the encoding of logical states, detection of single- and double-qubit errors, transversal Pauli logical operations, and a decoding circuit. We also verify the feasibility of error correction by measuring the ancillae of the decoded state.

The conventional circuit for encoding the logical state

$|\Psi\rangle_L$ requires a number of two qubit gates which are non-local with respect to a linear architecture [4, 5]. To tailor the circuit for superconducting systems that only involve nearest-neighbour controlled-phase gates, we recompile the encoding circuit to have the minimal possible number (eight) of nearest-neighbour control phase gates as shown in Fig. 1(a).

On a superconducting quantum processor [24, 25], we experimentally realised the logical states $|0\rangle_L, |1\rangle_L, |\pm\rangle_L$, and $|\pm i\rangle_L$ that are eigenstates of the logical Pauli operators X_L, Y_L , and Z_L , and the magic state $|T\rangle_L = (|0\rangle_L + e^{i\pi/4}|1\rangle_L)/\sqrt{2}$ that cannot be realized by applying Clifford operations on any eigenstate of the logical Pauli operators. The expectation values of the stabilizer operators of $|T\rangle_L$ is shown in Fig. 1(b), with all positive

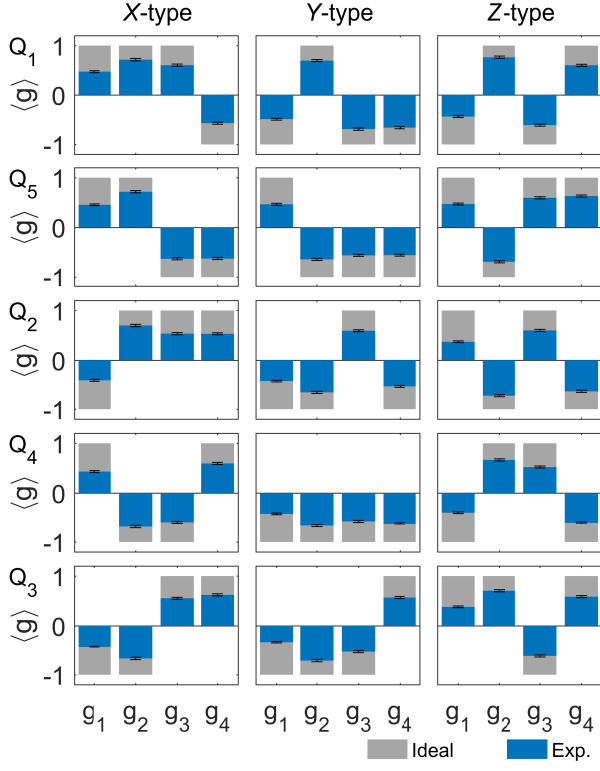


FIG. 2. Error correction on the logic magic state $|T\rangle_L$. A single-qubit X -, Z -, or Y -type error, which corresponds to bit-flip, phase-flip, or a combined error, respectively, is applied to one of the five qubits Q_1 to Q_5 . We destructively measure the four stabilizers and find consistent syndrome correlations that identify the quantum error.

values and state fidelity \mathcal{F}_L being 54.5(4)%. The fidelities of other prepared states are shown in Supplementary Materials, with an average fidelity being 57.1(3)%.

The quality of the prepared logical states can also be divided into its overlap with the logical code space and its agreement with the target logical state after projecting it into the code space. Given the logical Pauli operators X_L, Y_L, Z_L and $I_L = |0\rangle_L \langle 0|_L + |1\rangle_L \langle 1|_L$, the normalised density matrix ρ_L is defined by projecting the experimentally prepared state ρ_q into the code space

$$\rho_L = \frac{I + \bar{P}_X X_L + \bar{P}_Y Y_L + \bar{P}_Z Z_L}{2}, \quad (2)$$

with normalised probability $\bar{P}_j = P_j/P_I$ and $P_j = \text{Tr}(\rho_q j_L)$, for all $j = I, X, Y, Z$. We define the fidelity within the code space by $\mathcal{F}_L = \langle \Psi |_L \rho_L | \Psi \rangle_L$, as shown in Fig. 1(c), with the average value being as high as 99.3(1)%.

Given the realisation of logical state, one can proceed with the implementation of error correction/detection. Acting on the logical encoded state $|T\rangle_L$, we systematically introduce every type of single-qubit error by artificially applying the corresponding single qubit gate on

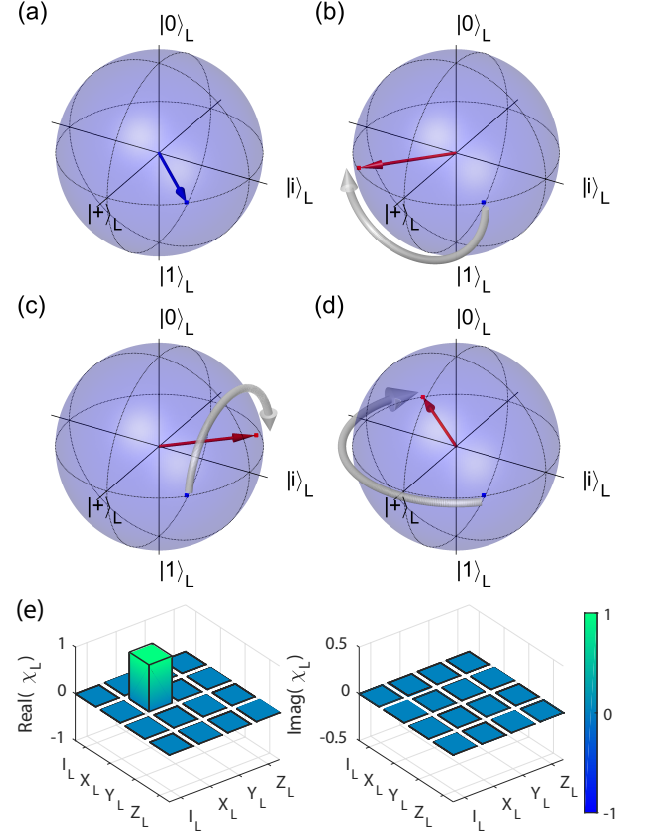


FIG. 3. Logical operation within the code space. (a) Encoded logical state $|T\rangle_L$ illustrated on the logical Bloch sphere. (b)-(d) Single logical-qubit operation X_L, Y_L and Z_L applied on $|T\rangle_L$. The blue squares and vector are the initial states. The red circles and vectors are the final states. The states are projected into the code space. The fidelities of the state after gate operation are 98.6(1)%, 98.0(1)% and 98.7(1)% for (b), (c), and (d), respectively. The white arrow illustrates the dynamics under the gate operation. (e) The χ_L matrix of the logical X_L operation determined via quantum process tomography in the code space. The gate fidelity of logical X_L operation is determined to be 97.2(2)%. The black-outlined hollow bars correspond to the ideal X gate. We refer to Supplementary Materials for the definition of the χ_L matrix and details.

one of the five qubits. Then, by measuring the four stabilizers g_1, g_2, g_3 , and g_4 , we aim to verify that each error would be properly identified. As shown in Fig. 2(a) we do indeed find, for each case, the exact syndrome pattern that identifies the location of the single-qubit error. We also apply double-qubit errors on $|T\rangle_L$ and find the same syndrome correlation that can always detect the existence of errors (see Supplementary Material for details). Notably, the (single-qubit or double-qubit) error-afflicted states have negligible probabilities projecting onto the code space (around 3.3%), verifying the power of error correction and detection.

In a functioning fault-tolerant quantum computer, op-

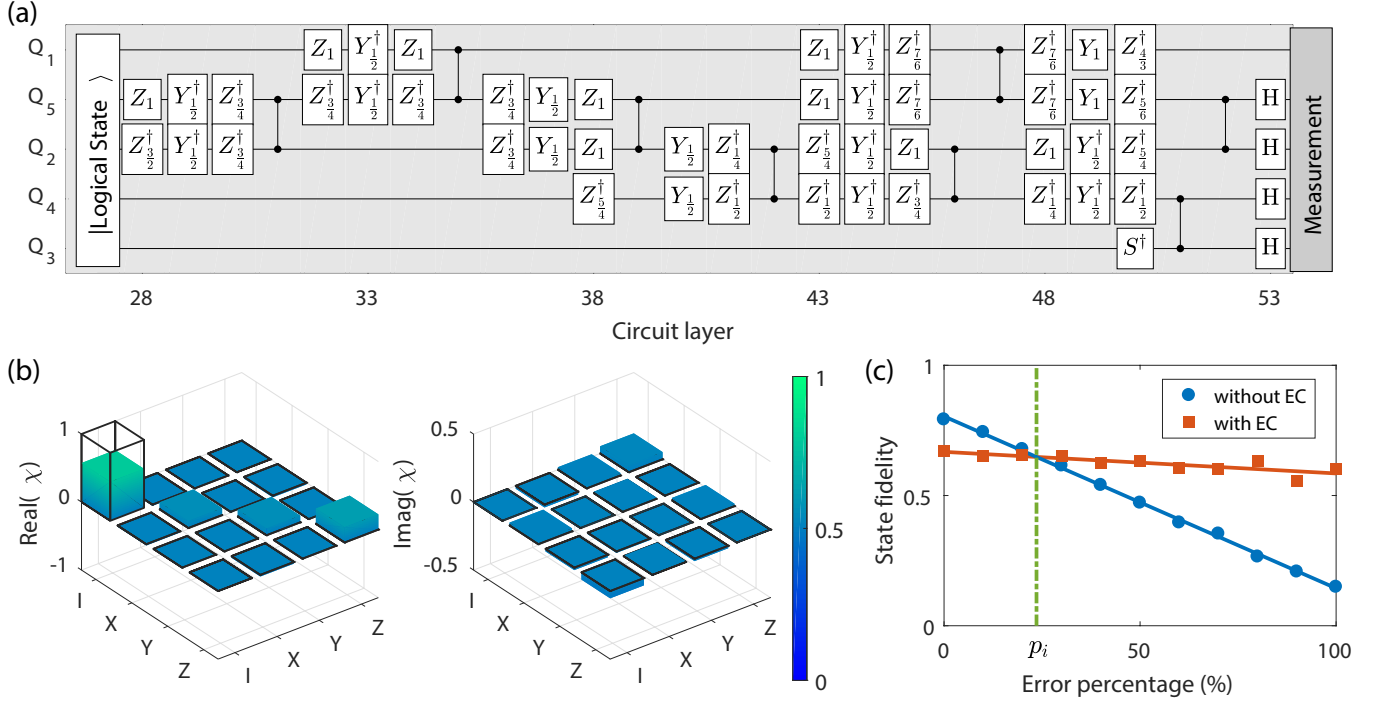


FIG. 4. Decoding of the five-qubit code. (a) The decoding quantum circuit is the inverse of the encoding circuit shown in Fig. 1(b) with opposite rotation angles. (b) The χ_L matrix of the encoding and decoding circuit. The fidelity of the whole process reaches 57.4(7)%. The black-outlined hollow bars correspond to the identical process. (c) Error correction of the decoded state. In general, a mixed state ρ_f with single-qubit error occurred with error percentage p can be described as $\rho_f = p\rho_E + (1-p)\rho_I$, where ρ_E and ρ_I are density matrices of the five-qubit state with and without error, respectively. In this experiment, to verify the capability of error correction of this code, we obtain ρ_E or ρ_I by introducing the single-qubit error via applying corresponding gate on one of the qubits or not; ρ_E and ρ_I are measured by performing quantum state tomography. For each error percentage, we measure the density matrices separately and then construct the mixed state ρ_f with each groups of ρ_E , ρ_I and p . After obtaining the reconstructed density matrix ρ_f , we identify the single-qubit error and mathematically recover the state. Here we show the logical $|0\rangle_L$ state with single-qubit Y -type error introduced on Q_1 , the state fidelity before and after error correction are presented in blue circles and red squares, respectively. The error estimated via bootstrapping is typically around 0.3% and smaller than the symbol size. After fitting the state fidelity before and after error correction as a linear function of error percentage, an intersection with error percentage $p_i = 23.6\%$ is obtained, shown in green dashed line. The cases with other types of single-qubit error can be found in Supplementary Materials.

erations on logical qubits are realised through a series of operations on the component physical qubits. We implement and verify three such transversal logical operations: Starting from the post-selected magic state $|T\rangle_L$ presented in Fig. 3(a), we demonstrate the single logical qubit operations X_L , Y_L , and Z_L , and plot the rotated states within the code space, as shown in Fig. 3(b), (c), and (d), respectively. To characterize these logical operations, we performed the quantum process tomography within the code space as shown in Figure 3(e), and determine gate fidelities of the logical X_L , Y_L , and Z_L operations as 97.2(2)%, 97.8(2)%, and 97.3(2)%, respectively.

Finally, we apply the decoding circuit, as shown in Fig. 4(a), to map the encoded state back to the input state, in total with 122 gates. With input states $|0\rangle$, $|1\rangle$, $|+\rangle$, and $|+i\rangle$, we determine the state fidelity after decoding as 77.7(6)%, 82.0(5)%, 64.1(7)%, and 66.4(7)%, respectively, and the whole process fidelity as 57.4(7)%,

shown in Fig. 4(b). Interestingly, when assuming ideal circuit decoding, any single qubit error can be uniquely identified by measuring the four ancillae (Q_2 - Q_5) in the computational basis. This error can further be corrected by applying a corresponding single qubit recovery operation on the decoded state, with details discussed in methods. As shown in Fig. 4(c), for logical $|0\rangle_L$ state with single-qubit Y -type error introduced on Q_1 , we compare the fidelities before and after error correction. For error percentage higher than $p_i = 23.6\%$, we verified that the state fidelity can be improved after mathematical error correction. Cases with other types of single-qubit errors and different logical states can be found in Supplementary Materials. We emphasize that, while genuine error correction can be realized in future experiments with high-fidelity single-shot measurements and real-time feedback, however here we simulate it with the reconstructed density matrix. In Supplementary Mate-

rials, we also realize the decoding process by only applying operations on the top three qubits. The fidelity of the encoding-decoding process with in total 93 gates is found to be 74.5(6)%. Our result also verifies the capability of quantum secret sharing with the five-qubit code [26].

An essential milestone on the road to fault-tolerant quantum computing is the achievement of error-corrected logical qubits that genuinely benefit from error correction, outperforming simple physical qubits. As this requires highly-accurate control of many qubits, and over a substantial number of gates, such a goal has remained a worldwide challenge for more than a decade. Our experiment completes the first and also the most important step towards this goal by realising the basic ingredients of a full functional five-qubit error correcting code. Combining theoretical advances in circuit optimization together with high-quality superconducting qubits, our work paves the way towards fault-tolerant quantum computing with continuing technological development.

ACKNOWLEDGMENTS

The authors thank the USTC Center for Micro- and Nanoscale Research and Fabrication, Institute of Physics CAS and National Center for Nanoscience and Technology for the support of the sample fabrication. The authors also thank QuantumCTek Co., Ltd. for supporting the fabrication and the maintenance of room temperature electronics. **Funding:** This work was supported by the National Key Research and Development Program of China (Grants No. 2017YFA0304300, No. 2017YFA0303900 and No. 2017YFA0304004), the National Natural Science Foundation of China (Grants No. 11875173, No. 11674193 and No. 11574380), the Chinese Academy of Science, Science and Technology Committee of Shanghai Municipality, and Anhui Initiative in Quantum Information Technologies. SCB and XY acknowledge EPSRC grant EP/M013243/1.

-
- [1] Gottesman, D. Theory of fault-tolerant quantum computation. *Phys. Rev. A* **57**, 127–137 (1998).
 - [2] Shor, P. W. Scheme for reducing decoherence in quantum computer memory. *Phys. Rev. A* **52**, R2493–R2496 (1995).
 - [3] Steane, A. M. Error correcting codes in quantum theory. *Phys. Rev. Lett.* **77**, 793–797 (1996).
 - [4] Bennett, C. H., DiVincenzo, D. P., Smolin, J. A. & Wootters, W. K. Mixed-state entanglement and quantum error correction. *Phys. Rev. A* **54**, 3824–3851 (1996).
 - [5] Laflamme, R., Miquel, C., Paz, J. P. & Zurek, W. H. Perfect quantum error correcting code. *Phys. Rev. Lett.* **77**, 198–201 (1996).
 - [6] Reed, M. D. *et al.* Realization of three-qubit quantum error correction with superconducting circuits. *Nature* **482**, 382 (2012).
 - [7] Nigg, D. *et al.* Quantum computations on a topologically encoded qubit. *Science* 1253742 (2014).
 - [8] Waldherr, G. *et al.* Quantum error correction in a solid-state hybrid spin register. *Nature* **506**, 204 (2014).
 - [9] Shor, P. W. Algorithms for quantum computation: discrete logarithms and factoring. In *Proceedings 35th Annual Symposium on Foundations of Computer Science*, 124–134 (1994).
 - [10] Lloyd, S. Universal quantum simulators. *Science* 1073–1078 (1996).
 - [11] Knill, E. Quantum computing with realistically noisy devices. *Nature* **434**, 39 (2005).
 - [12] Aliferis, P., Gottesman, D. & Preskill, J. Quantum accuracy threshold for concatenated distance-3 codes. *Quantum Info. Comput.* **6**, 97–165 (2006).
 - [13] Lu, C.-Y. *et al.* Experimental quantum coding against qubit loss error. *Proceedings of the National Academy of Sciences* **105**, 11050–11054 (2008).
 - [14] Yao, X.-C. *et al.* Experimental demonstration of topological error correction. *Nature* **482**, 489 (2012).
 - [15] Bell, B. *et al.* Experimental demonstration of a graph state quantum error-correction code. *Nature communications* **5**, 3658 (2014).
 - [16] Chiaverini, J. *et al.* Realization of quantum error correction. *Nature* **432**, 602 (2004).
 - [17] Schindler, P. *et al.* Experimental repetitive quantum error correction. *Science* **332**, 1059–1061 (2011).
 - [18] Linke, N. M. *et al.* Fault-tolerant quantum error detection. *Science advances* **3**, e1701074 (2017).
 - [19] Kelly, J. *et al.* State preservation by repetitive error detection in a superconducting quantum circuit. *Nature* **519**, 66 (2015).
 - [20] Ofek, N. *et al.* Extending the lifetime of a quantum bit with error correction in superconducting circuits. *Nature* **536**, 441 (2016).
 - [21] Takita, M., Cross, A. W., Córcoles, A. D., Chow, J. M. & Gambetta, J. M. Experimental demonstration of fault-tolerant state preparation with superconducting qubits. *Phys. Rev. Lett.* **119**, 180501 (2017).
 - [22] Taminiau, T. H., Cramer, J., van der Sar, T., Dobrovitski, V. V. & Hanson, R. Universal control and error correction in multi-qubit spin registers in diamond. *Nature nanotechnology* **9**, 171 (2014).
 - [23] Cramer, J. *et al.* Repeated quantum error correction on a continuously encoded qubit by real-time feedback. *Nature communications* **7**, 11526 (2016).
 - [24] Gong, M. *et al.* Genuine 12-Qubit Entanglement on a Superconducting Quantum Processor. *Physical Review Letters* **122**, 110501 (2019).
 - [25] Yan, Z. *et al.* Strongly correlated quantum walks with a 12-qubit superconducting processor. *Science* **364**, 753–756 (2019).
 - [26] Cleve, R., Gottesman, D. & Lo, H.-K. How to share a quantum secret. *Phys. Rev. Lett.* **83**, 648–651 (1999).

METHODS

Five-qubit error correction The five-qubit code has distance three and therefore all single-qubit errors can be identified (and thus corrected) while all double-qubit errors can be detected. When there is no error, all stabilizer measurements should yield +1 for the encoded state $|\Psi\rangle_L$. When an error happens, one or more stabilizer measurements may yield -1. As there are four stabilizers whose measurement may take either +1 or -1 values, there are in total 15 syndrome measurement results with at least one outcome being -1. If we consider the ways in which a single Pauli error can afflict one of the five qubits, we note that there are fifteen possibilities (three error types and five locations), with each mapping to a specific one of the fifteen syndromes. When a two-qubit error happens, we again find that at least one of the stabilizer measurements takes -1. This heralds the fact that some error has occurred. However, since different double-qubit errors may have the same syndrome, we can only detect double-qubit errors without the capability of identifying or correcting them. Nevertheless, this latter property can be useful in some situations, such as state preparation, where we can simply discard a faulty realisation and restart.

Experimental set-up The device for the implementation of the five-qubit error correcting code is a 12-qubit superconducting quantum processor [24, 25]. Among these 12 qubits, we chose five adjacent qubits to perform the experiment. The qubits are capacitively coupled to their nearest neighbours. The capacitively coupled XY control lines enable the application of single-

qubit rotation gates by applying microwave pulses, and the inductively coupled Z control lines enable the double-qubit controlled-phase gates by adiabatically tune the two-qubit state $|11\rangle$ close to the avoid level crossing of $|11\rangle$ and $|02\rangle$ [24]. After careful calibration and gate optimization, we have the average gate fidelities as high as 0.9993 for single-qubit gates and 0.986 for two-qubit gates. With the implementation of only single-qubit rotation gates and double-qubit controlled-phase gates, we realized the circuit for encoding and decoding of the logical state. More details about the experimental set-up are shown in Supplementary Materials.

Error correction after decoding Denote the encoding and decoding circuit channels as \mathcal{U} and \mathcal{U}^\dagger , respectively. When no error happens, we can recover the input state by encoding and then decoding, i.e., $\mathcal{U}^\dagger \circ \mathcal{U} \left(|\Psi\rangle |0\rangle^{\otimes 4} \right) = |\Psi\rangle |0\rangle^{\otimes 4}$ with single qubit states $|\Psi\rangle = a|0\rangle + b|1\rangle$ and computational basis $\{|0\rangle, |1\rangle\}$. When errors \mathcal{E} happen after the encoding circuit, the state after decoding is generally different from $|\Psi\rangle |0\rangle^{\otimes 4}$. In particular, when \mathcal{E} corresponds to a single qubit Pauli error, the output state is in general $\mathcal{U}^\dagger \circ \mathcal{E} \circ \mathcal{U} \left(|\Psi\rangle |0\rangle^{\otimes 4} \right) = \mathcal{E}_x(|\Psi\rangle) |x\rangle$, with a single qubit Pauli error \mathcal{E}_x uniquely determined by the value $x \in \{0, 1, \dots, 15\}$ of the four ancillae. Therefore, by measuring the ancillae in the computational basis, we can uniquely identify any single qubit error \mathcal{E} of the encoded state. We can further correct it by decoding the state and applying the recovery operation that corrects the induced single qubit error \mathcal{E}_x on the decoded state. We leave the syndrome table of $\{x, \mathcal{E}_x\}$ in Supplementary Materials. The experimental verification can be found in Fig. 4.

Supplementary Information for “Experimental verification of five-qubit quantum error correcting with superconducting qubits”

(Dated: June 27, 2022)

CONTENTS

I. Theory	1
A. Code description	1
B. Fidelity evaluation	2
C. Error detection and correction	3
D. Encoding circuit	3
II. Experiment	5
A. Device	5
B. Implementation of quantum circuit	5
C. Logical state preparation	6
D. Two-qubit error detection	6
E. Logical gate operations	7
F. Error correction after decoding	8
G. Energy relaxation of the logical qubit	10
H. Decoding three qubits	10
References	11

I. THEORY

A. Code description

The five-qubit quantum error correcting code (QECC) maps an input state $|\phi\rangle = a|0\rangle + b|1\rangle$ to a five-qubit state, $|\Psi\rangle_L = a|0\rangle_L + b|1\rangle_L$, where the logical $|0\rangle_L$ and $|1\rangle_L$ states are defined by

$$\begin{aligned}
 |0\rangle_L &= \frac{1}{4} [|00000\rangle + |10010\rangle + |01001\rangle + |10100\rangle \\
 &\quad + |01010\rangle - |11011\rangle - |00110\rangle - |11000\rangle \\
 &\quad - |11101\rangle - |00011\rangle - |11110\rangle - |01111\rangle \\
 &\quad - |10001\rangle - |01100\rangle - |10111\rangle + |00101\rangle], \\
 |1\rangle_L &= \frac{1}{4} [|11111\rangle + |01101\rangle + |10110\rangle + |01011\rangle \\
 &\quad + |10101\rangle - |00100\rangle - |11001\rangle - |00111\rangle \\
 &\quad - |00010\rangle - |11100\rangle - |00001\rangle - |10000\rangle \\
 &\quad - |01110\rangle - |10011\rangle - |01000\rangle + |11010\rangle].
 \end{aligned} \tag{S1}$$

The five-qubit code is a stabilizer code [1], which is defined by a set of independent operators from the Pauli group that have eigenvalues ± 1 . The stabilizer operators of the five-qubit code together with its logical Pauli operators are listed in Table S1.

The logical state space is defined by states $|\Psi\rangle_L = a|0\rangle_L + b|1\rangle_L$ which are simultaneously stabilized by the four stabilizers with $g_i|\Psi\rangle_L = +|\Psi\rangle_L$, $\forall i = 1, 2, 3, 4$. Logical Pauli operators can be transversally realised by applying the corresponding operation separately on each physical qubit. The logical states $|0\rangle_L$ and $|1\rangle_L$ are eigenstates of the logical Z_L operator. General logical operators, such as the $T_L = e^{-iZ_L\pi/8}$ gate, the Hadamard gate H_L , may not be transversally realised.

TABLE S1. The stabilizer generators of the five-qubit code and the logical Z_L , X_L , and Y_L operations. Here I_i , X_i , Y_i , Z_i are the Pauli matrices acting on the i^{th} qubit.

Name	Operator
g_1	$X_1 Z_2 Z_3 X_4 I_5$
g_2	$I_1 X_2 Z_3 Z_4 X_5$
g_3	$X_1 I_2 X_3 Z_4 Z_5$
g_4	$Z_1 X_2 I_3 X_4 Z_5$
\bar{X}	$X_1 X_2 X_3 X_4 X_5$
\bar{Z}	$Z_1 Z_2 Z_3 Z_4 Z_5$
\bar{Y}	$Y_1 Y_2 Y_3 Y_4 Y_5$

B. Fidelity evaluation

The logical state $|\Psi\rangle_L = a|0\rangle_L + b|1\rangle_L$ can be uniquely determined by the four stabilizers defined in Table S1 together with the fifth stabilizer

$$\begin{aligned}
g_5 &= |\Psi\rangle\langle\Psi| - |\Psi^\perp\rangle\langle\Psi^\perp| \\
&= (a|0\rangle_L + b|1\rangle_L)(a^*\langle 0|_L + b^*\langle 1|_L) - (b^*|0\rangle_L - a^*|1\rangle_L)(b\langle 0|_L - a\langle 1|_L) \\
&= (aa^* - bb^*)(|0\rangle_L\langle 0|_L - |1\rangle_L\langle 1|_L) + 2a^*b|1\rangle_L\langle 0|_L + 2b^*a|0\rangle_L\langle 1|_L \\
&= (aa^* - bb^*)Z_L + (a^*b + b^*a)X_L - i(a^*b - b^*a)Y_L.
\end{aligned} \tag{S2}$$

with $|\Psi^\perp\rangle = b^*|0\rangle_L - a^*|1\rangle_L$. That is, any logical state $|\Psi\rangle_L$ can be decomposed as

$$|\Psi\rangle_L\langle\Psi|_L = \frac{1}{2^5} \prod_{i=1}^5 (g_0 + g_i), \tag{S3}$$

where $g_0 = I_1 I_2 I_3 I_4 I_5$. Therefore the fidelity between the experimentally prepared state ρ_q and the ideal target state $|\Psi\rangle_L\langle\Psi|_L$ can be also determined by the measurement of the 32 stabilizer operators $\prod_{i=1}^5 (g_0 + g_i)$. That is,

$$\mathcal{F} = \langle\Psi|_L \rho_q |\Psi\rangle_L = \sum_j \text{tr}[\rho_q g_j], \tag{S4}$$

where g_j is one of the 32 terms by expanding $\prod_{i=1}^5 (g_0 + g_i)$.

The fidelity of the prepared logical states can also be divided into its overlap with the logical code space and its agreement with the target logical state after projecting it into the code space. Given the logical Pauli operators,

$$\begin{aligned}
X_L &= |+\rangle_L\langle +|_L - |-\rangle_L\langle -|_L, \\
Y_L &= |+\rangle_L\langle +i|_L - |-\rangle_L\langle -i|_L, \\
Z_L &= |0\rangle_L\langle 0|_L - |1\rangle_L\langle 1|_L, \\
I_L &= |0\rangle_L\langle 0|_L + |1\rangle_L\langle 1|_L,
\end{aligned} \tag{S5}$$

with $|\pm\rangle_L = (|0\rangle_L \pm |1\rangle_L)/\sqrt{2}$ and $|\pm i\rangle_L = (|0\rangle_L \pm i|1\rangle_L)/\sqrt{2}$, the normalised density matrix ρ_L is defined by projecting ρ_q into the code space

$$\rho_L = \frac{I + \bar{P}_X X_L + \bar{P}_Y Y_L + \bar{P}_Z Z_L}{2}, \tag{S6}$$

with normalised probability $\bar{P}_j = P_j/P_I$ and $P_j = \text{Tr}(\rho_q j_L)$, for all $j = I, X, Y, Z$. After projecting ρ_q into the code space, we define the fidelity within the code space by

$$\mathcal{F}_L = \langle\Psi|_L \rho_L |\Psi\rangle_L. \tag{S7}$$

C. Error detection and correction

The five-qubit code has a distance three, and therefore any single-qubit or two-qubit errors will be detected by a stabilizer change, and single-qubit errors can be successfully corrected (while if the correction protocol were applied to a two-qubit error state, a logical error would result). When there is no error, the stabilizers are all 1 for the encoded state $|\Psi\rangle_L$. When error happens, the stabilizers may have negative values. As there are four stabilizers either taking ± 1 values, there are in total 15 syndrome measurement results with at least one stabilizer value being negative. For each one of the 15 cases with one single qubit error happens on one of the five qubits, it corresponds to a unique syndrome. When a two-qubit error happens, one of the stabilizers must take a negative value, indicating the existence of errors. As different two-qubit errors may have the same syndrome (degeneracy), we can only detect two-qubit errors without the capability of correcting them.

D. Encoding circuit

In our experiment, we also consider the case where we relabel the code by mapping the original labels of the qubits as follows,

$$1' = 1, 2' = 5, 3' = 2, 4' = 4, 5' = 3. \quad (S8)$$

The four stailizers of the relabllled code are summarized in Table S2.

TABLE S2. The stabilizer generators of the relabelled five-qubit QECC code..

Name	Operator
g_1	$X_1 Z_2 Z_3 X_4 I_5 = X_{1'} I_{2'} Z_{3'} X_{4'} Z_{5'}$
g_2	$I_1 X_2 Z_3 Z_4 X_5 = I_{1'} X_{2'} X_{3'} Z_{4'} Z_{5'}$
g_3	$X_1 I_2 X_3 Z_4 Z_5 = X_{1'} Z_{2'} I_{3'} Z_{4'} X_{5'}$
g_4	$Z_1 X_2 I_3 X_4 Z_5 = Z_{1'} Z_{2'} X_{3'} X_{4'} I_{5'}$

The encoding circuit of the conventional five-error correction code is shown in Fig. S1. We manually searched this circuit so that minimal number of Controlled-Not (CNOT) gates is used. Here the gates that are used in the circuit are defined as

$$H = \frac{1}{\sqrt{2}} \begin{bmatrix} 1 & 1 \\ 1 & -1 \end{bmatrix}, S = \begin{bmatrix} 1 & 0 \\ 0 & i \end{bmatrix}, X = \begin{bmatrix} 0 & 1 \\ 1 & 0 \end{bmatrix}, Z = \begin{bmatrix} 1 & 0 \\ 0 & -1 \end{bmatrix}. \quad (S9)$$

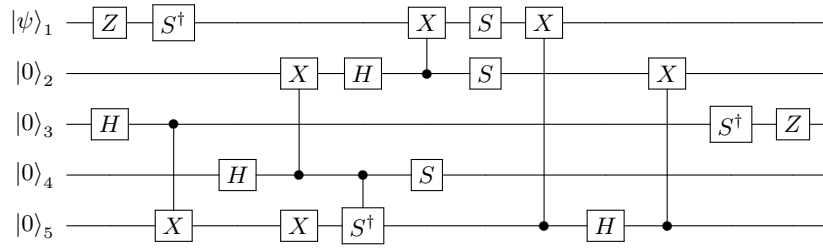


FIG. S1. Encoding circuit for the five-qubit error correction code. Qubit 1 is the unknown to-be encoded state $a|0\rangle + b|1\rangle$ and qubit 2 to 5 are the ancillae $|0\rangle$.

In our experiment, we relabel the qubits from 1, 2, 3, 4, 5 to $1', 3', 5', 4', 2'$ in order to make the nonlocal gates to be nearest-neighbour gates. By reordering the qubits as $1', 2', 3', 4', 5'$, we obtain the encoding circuit that only involves 6 nearest-neighbour gates and 2 swap gates, shown in Fig. S2. Each swap gate can be realized with 3 CNOT gates. The total number of nearest-neighbour CNOT gates are 12. It is worth noting that relabelling or reordering the ancillary qubits do not affect the code. The code is equivalent simply with stabilizers and all other measurement reordered.

Furthermore, we show that the number of nearest-neighbour CNOT gates can be reduced to 8 by numerically optimising the circuit. This is achieved by focusing on two clusters of gates in the two dashed boxes. As shown in

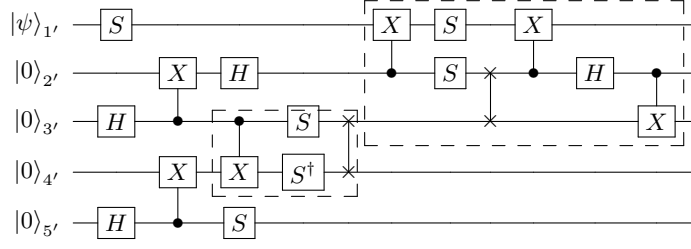


FIG. S2. Encoding circuit for the relabelled five-qubit error correction code.

Fig. S3, we recompile these two clusters of gates by replacing the swap gate with the Control-Z (CZ) gate and in the meanwhile inserting more parameterized single qubit gates. For each single qubit gate, we decompose it as

$$U_i = R_z(\alpha_i)R_y(\beta_i)R_z(\gamma_i), \quad (\text{S10})$$

with $R_z(\alpha) = e^{-i\alpha\sigma_z/2}$ and $R_y(\alpha) = e^{-i\alpha\sigma_y/2}$. We also add a parameter to the unitary to represent its global phase. Suppose the target unitary is U and the parameterised compiled circuit is $U(\vec{\theta})$, with $\vec{\theta}$ denoting all the parameters. Then we need to minimise the distance between U and $U(\vec{\theta})$

$$\min_{\vec{\theta}} \|U(\vec{\theta}) - U\|, \quad (\text{S11})$$

where $\|U\| = \sum_{i,j} |U_{i,j}|^2$. We numerically optimise the distance over all the parameters and we find that the circuits of the two dashed boxes can be simplified as desired with four CZ or CNOT gates reduced.

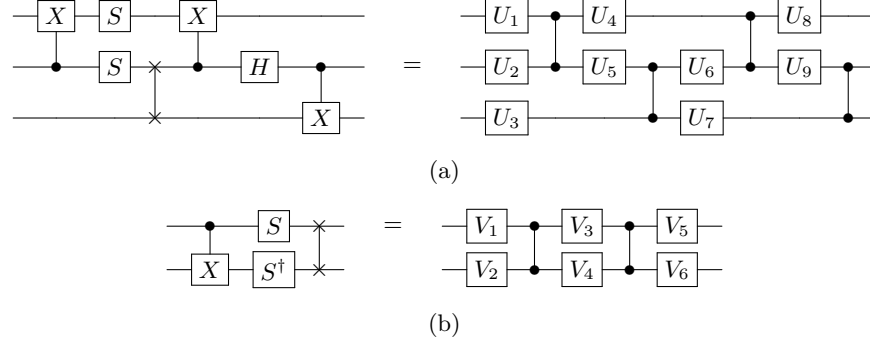


FIG. S3. Quantum circuit compilation. We recompile the two small circuits by fixing its structure with several parameterized single qubit gates. We replace the swap gate with the CZ gate and add general single qubit gates between every two CZ gates. Each single qubit gate has three parameters and we also add a global phase to the whole circuit. Circuit (a) has 28 parameters and Circuit (b) has 19 parameters. We perform the numerical optimization with the MATLAB *fminsearch* function, which realized the simulated annealing algorithm. As the parameter space is quite large, we run the algorithm with random initial parameters and find a local minimum at each time. We end the search until the distance is minimized that is below a certain threshold, say 10^{-3} . In practice, we only need to try tens of random initial parameters to find the global minimum. In general, the found rotation angles are not the exact fractional number as shown in Fig. S4 owing to numerical accuracy. We manually replace the rotation angles with the closest fractional numbers and verify the compiled circuit by obtaining negligible distance, say 10^{-10} .

After compiling the circuit and combining single qubit gates, we obtain our final encoding circuit as shown in Fig. S4.

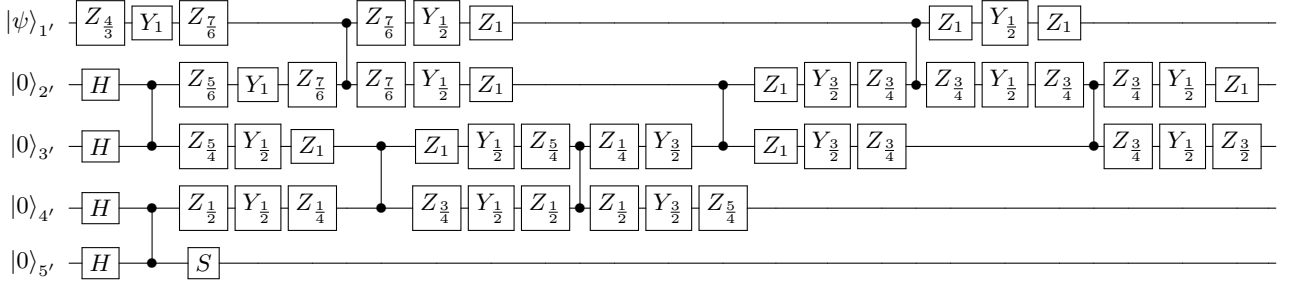


FIG. S4. Encoding circuit for the five qubit error correction code. Here $X_\alpha = e^{-i\alpha\sigma_x/2}$, $Y_\alpha = e^{-i\alpha\sigma_y/2}$, and $Z_\alpha = e^{-i\alpha\sigma_z/2}$ with Pauli matrices σ_x , σ_y , and σ_z .

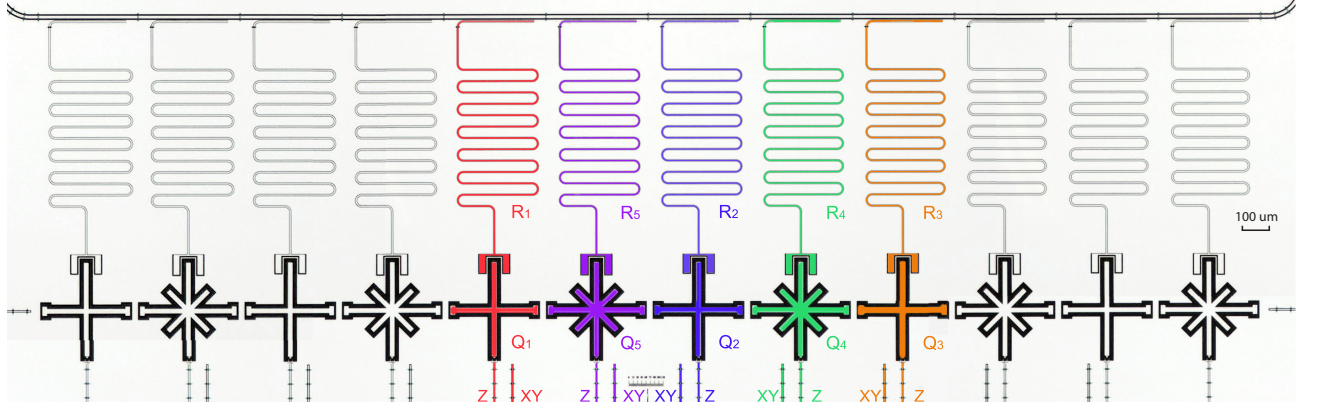


FIG. S5. Optical image of the superconducting quantum processor. There are in total 12 qubits, from which we choose five adjacent qubits labelled with Q_1 to Q_5 to perform the experiment. Each qubit couples to a corresponding resonator for state readout.

II. EXPERIMENT

A. Device

The device we used is a superconducting quantum processor. As illustrated in Fig. S5, there are 12 transmon qubits of the Xmon variety [2–4] arranged a 1D chain [5]. All qubits are frequency-tunable by their corresponding Z control lines. Each qubit couples to its nearest-neighbour qubits via fixed capacitors. The nearest-neighbour coupling strength is about 12 MHz. For each qubit, individual XY and Z control lines enable the ability to fully control the qubit state. Each qubit couples to a $\lambda/4$ resonator for state readout. All twelve resonators couple to a common transmission line. Among these qubits, we choose five high-quality adjacent qubits, labelled from Q_1 to Q_5 in Fig. S5, to perform the experiment. The performances of the qubits are listed in Table. S3. The relaxation time T_1 ranges from $27.5 \mu\text{s}$ to $48.6 \mu\text{s}$. The dephasing time T_2^* ranges from $2.7 \mu\text{s}$ to $5.6 \mu\text{s}$. To reduce the ZZ coupling between the neighboring qubits, the idle frequencies of the qubits alternate in a zigzag pattern. The minimum frequency difference between neighboring qubits is 740 MHz.

B. Implementation of quantum circuit

The controlled-phase gates used in our experiment is the fast adiabatic CZ gates [3, 6], realized by tuning the two qubit $|11\rangle$ state close to the avoid-crossing of $|11\rangle$ and $|02\rangle$ state following an adiabatic trajectory. The single-qubit rotation gates around X- or Y-axis are realized by applying Gaussian-enveloped microwave pulses through the XY control lines. A derivative reduction by adiabatic gate (DRAG) [7] protocol is used to reduce the phase error and state leakage to the second excited state in the application of single qubit gates. Note that for the realization of the single-qubit rotation gates around the Z-axis, i.e., $R_z(\theta)$, we shift the phase of the reference for a certain angle θ

Qubit	Q ₁	Q ₅	Q ₂	Q ₄	Q ₃	AVG.
$\omega_{10}/2\pi$ (GHz)	5.124	4.266	5.006	4.134	4.884	-
T_1 (μs)	27.5	34.0	33.0	36.8	48.6	36.0
T_2^* (μs)	5.5	4.1	5.6	2.7	3.3	4.2
f_{00}	0.982	0.932	0.931	0.934	0.963	0.945
f_{11}	0.831	0.874	0.885	0.899	0.916	0.872
X/2 gate fidelity	0.9994	0.9994	0.9992	0.9993	0.9993	0.9993
CZ gate fidelity	0.980	0.990	0.984	0.988		0.986

TABLE S3. Performance of qubits. ω_{10} is idle points of the qubits. T_1 and T_2^* are the energy relaxation time and dephasing time, respectively. f_{00} (f_{11}) is the possibility of correctly readout of qubit state in $|0\rangle$ ($|1\rangle$) after successfully initialized in $|0\rangle$ ($|1\rangle$) state. X/2 gate fidelity and CZ gate fidelity are single- and two-qubit gate fidelities obtained via performing randomized benchmarking.

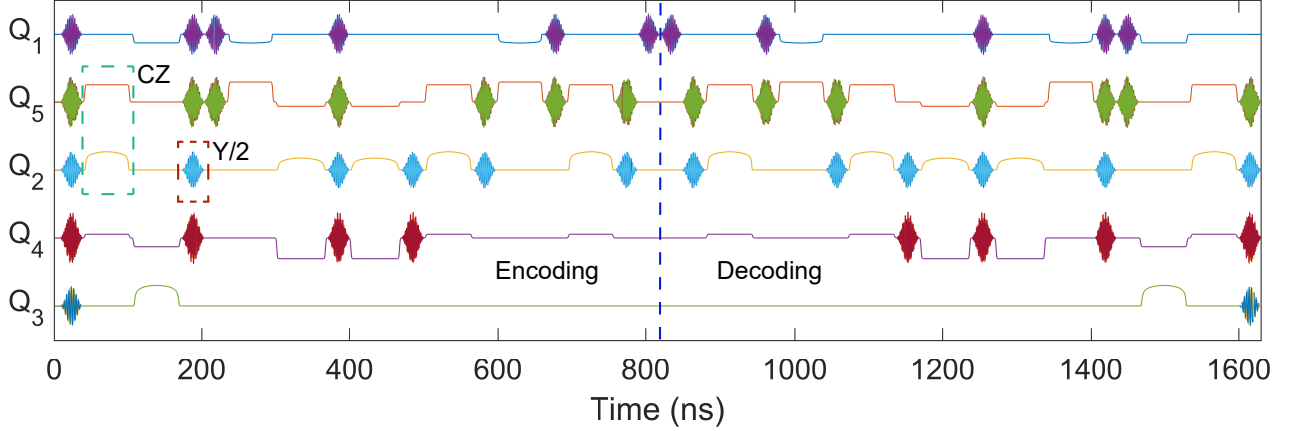


FIG. S6. Experimental waveform sequences for the implementation of encoding-decoding process. A typical CZ gate and a Y/2 gate are marked in the green and red dashed boxes, respectively. The blue dashed line marks the joint between encoding and decoding processes.

instead of applying a physical detuning pulse. The single- and double-qubit gate fidelities, determined via randomized benchmarking (RB), are listed in Table. S3, with the average fidelity obtained as 99.93% and 98.6%, respectively. The experimental waveform sequences are shown in Fig. S6. The evolution time for both encoding and decoding processes are about 810 ns. For each result measured in our experiment, we repeat the waveform sequences and state readout for 5,000 to 10,000 times.

C. Logical state preparation

We prepare seven logical states, including the six eigenstates $|0\rangle_L$, $|1\rangle_L$, $|+\rangle_L = (|0\rangle_L + |1\rangle_L)/\sqrt{2}$, $|-\rangle = (|0\rangle_L - |1\rangle_L)/\sqrt{2}$, $|+i\rangle = (|0\rangle_L + i|1\rangle_L)/\sqrt{2}$, and $|-i\rangle = (|0\rangle_L - i|1\rangle_L)/\sqrt{2}$ of the Pauli matrices and the magic state $|T\rangle_L = (|0\rangle_L + e^{i\pi/4}|1\rangle_L)/\sqrt{2}$. The results are shown in Table S4, where the raw state fidelities are determined as the fidelity between the experimentally obtained density matrix and that of the ideal state. Focusing on states in the code space, the state fidelity can be enhanced from 55.3% to 98.6% on average. The probability of projecting the state to the code space is 56.2%, which is close to the raw state fidelity after multiplying the fidelity in the code space. The expectation values of logical Pauli operators and the state fidelity of the magic state $|T\rangle_L$ are shown in Fig. 1 (c) in main text. The results for the other six states are shown in Fig. S7.

D. Two-qubit error detection

The result of single qubit error identification is shown in the main text. We found that the measured syndrome correlation can uniquely determine the artificially introduced single error. To check the two-qubit error detection

TABLE S4. Fidelity of the prepared logical states. The state fidelity within code space is equivalent to the one of the state after post-selecting +1 stabilizer measurement outcomes. The uncertainties are estimated via bootstrapping.

Logical state	$ 0\rangle_L$	$ 1\rangle_L$	$ +\rangle_L$	$ -\rangle_L$	$ +i\rangle_L$	$ -i\rangle_L$	$ T\rangle_L$	AVG.
State fidelity from state tomography	0.567(3)	0.533(3)	0.527(3)	0.581(3)	0.594(3)	0.547(3)	0.524(4)	0.553(3)
State fidelity from stabilizers	0.586(3)	0.551(3)	0.541(3)	0.598(3)	0.612(3)	0.564(3)	0.545(4)	0.571(3)
State fidelity within code space	0.984(1)	0.988(1)	0.982(1)	0.990(1)	0.987(1)	0.975(1)	0.993(1)	0.986(1)
Post-selection probability	57.6%	54.0%	53.6%	58.7%	60.2%	56.2%	53.2%	56.2%

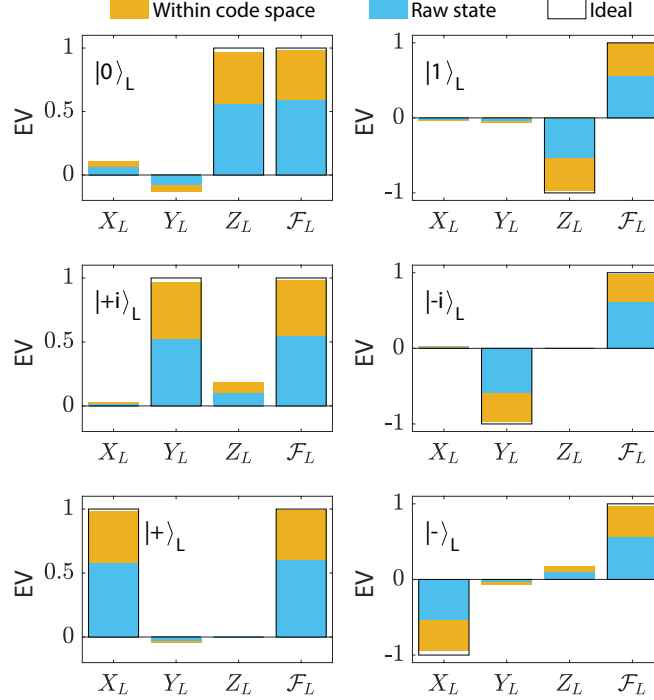


FIG. S7. Expectation values of logical Pauli operators and state fidelity of logical states. The six prepared states are $|0\rangle_L$, $|1\rangle_L$, $|+i\rangle_L$, $|-i\rangle_L$, $|+\rangle_L$, and $|-\rangle_L$, respectively. In each plot, logical Pauli expectation values and the state fidelity for the ideal state, raw experiment states, and states within the code space are shown in black-outlined hollow, blue, and brown bars, respectively.

with the five-qubit error correction code, we firstly prepared the logical encoded state $|T_L\rangle$. Then, by applying two single-qubit gates on two of the five qubits, we introduce artificial two-qubit errors. The single-qubit gates are chosen from the X , Z and Y gates. We measured the four stabilizer operators g_1 , g_2 , g_3 , and g_4 , and realized the error detection of the two-qubit error. The exact syndrome indicates that the existence of two-qubit errors can be exactly detected. The results are shown in Fig. S8.

E. Logical gate operations

The fidelity of logical gate operations are determined by performing quantum process tomography (QPT) [8, 9] of the corresponding operations. The χ matrix determined in QPT is defined as $\varepsilon(\rho) = \sum E_m \rho E_n^\dagger \chi_{mn}$, where ε is the quantum operation, ρ is the density matrix of the input state, and E_m 's are the operation bases, which in our case corresponds to $\{I, \sigma_x, -i\sigma_y, \sigma_z\}$. We prepare 4 input states of Q_1 in total, i.e. $|0\rangle$, $|1\rangle$, $|+\rangle$, and $|+i\rangle$, and measure the quantum state tomography (QST) of the output state of Q_1 with each input state. For each quantum state tomography components, we repeat the gate sequences and measurement for 5,000 times. After correcting the measurement error of QST with maximum-likelihood estimation, we reconstruct the 4×4 experimental χ matrix from the 4 density matrices. The process fidelity is determined as the trace overlap between the χ matrices of the ideal

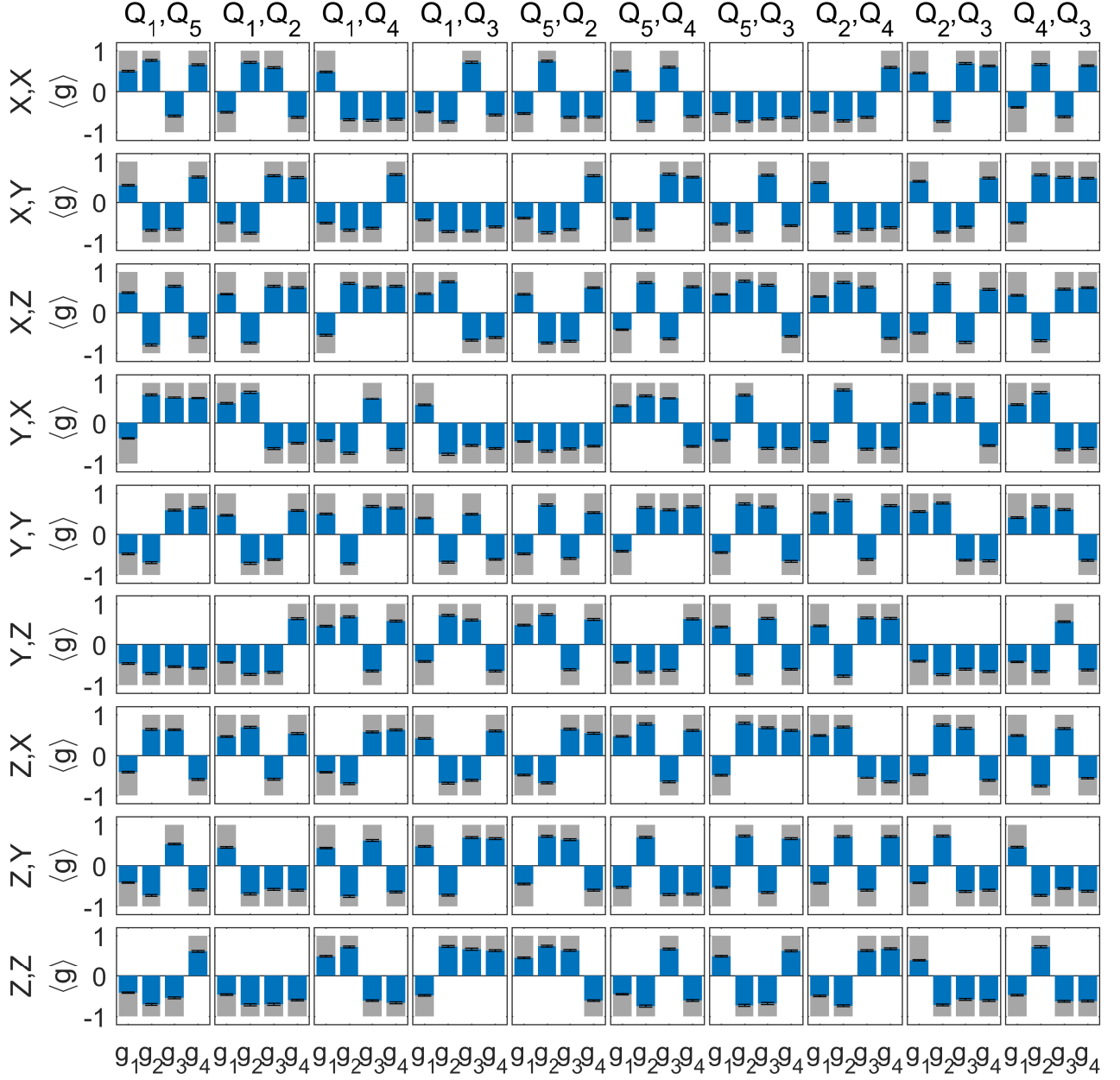


FIG. S8. Two-qubit error detection. Each column corresponds to a type of two-qubit error, and each row corresponds to a set of qubits error happened. The exact syndrome patterns indicate the ability of detecting double-qubit errors.

process and that obtained from QPT. The raw gate fidelities are determined to be 86.8%, 87.2%, and 86.1%, for X_L , Y_L , and Z_L , respectively. Instead, we can also consider gate fidelities only in the code space. For each state tomography, we extract the density matrix of the state within the code space. For Y_L and Z_L , the gate fidelities in the code space are determined to be 97.8(2)% and 97.3(2)%, respectively. The results are shown in Fig. S9.

F. Error correction after decoding

After the decoding process, the four ancillary qubits (Q_2 - Q_5) can be used to uniquely identify single-qubit errors occurred before the decoding circuit. We present the syndrome table of the relationship between the single qubit error and the four ancillae in Table S5. Ideally, we can destructively measure the ancillae, determine the error type, and apply a corresponding recovery operation to correct the induced error on the decoded qubit. However, this requires

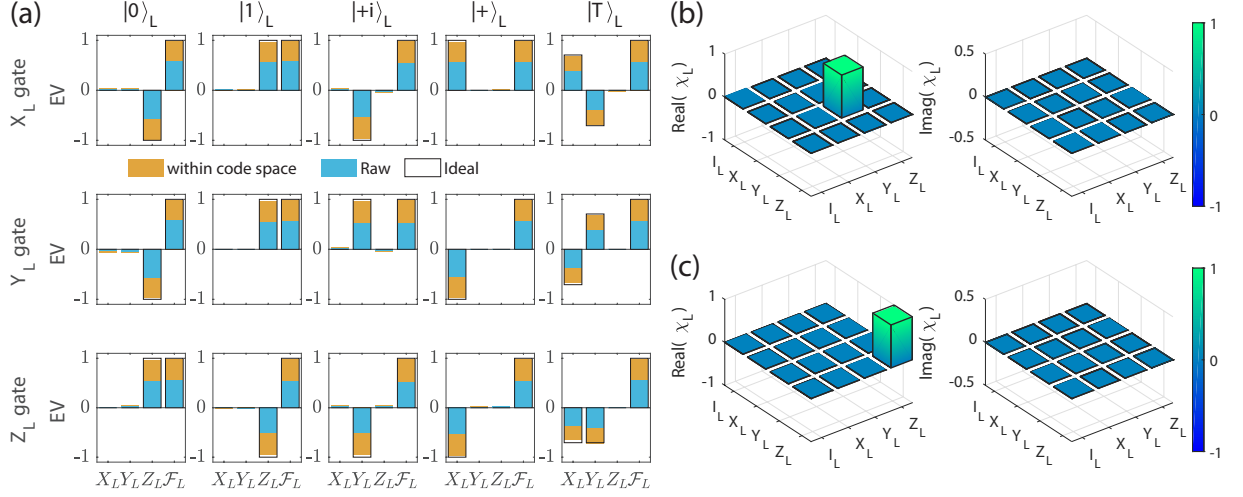


FIG. S9. (a) Expectation values of three logical Pauli operators and the state fidelity of the five initial logical states after the corresponding logical qubit operation, X_L , Y_L , and Z_L , respectively. The five logical states are $|0\rangle_L$, $|1\rangle_L$, $|+\rangle_L$, $|+i\rangle_L$, $|T\rangle_L$, respectively. For each gate operation, the state tomography with the first four initial states are used to obtain the χ_L matrix of the process. In each figure, logical qubit density matrix determined with post-selection, without post-selection, and that of the ideal state, are shown in brown, blue, and black outlined hollow bars, respectively. (b) and (c) Quantum process tomography of logical operations Y_L and Z_L , respectively. The logical qubit density matrices are determined with post-selection. The process fidelities are 97.8(2)% and 97.3(2)%, respectively. The black-outlined hollow bars correspond to the ideal process.

accurate single-shot measurements and realization of feedforward operations, which are not available in our current hardware. Nevertheless, we can still verify the capability of error correction. We prepare an encoded logical state and apply a single-qubit error gate before the decoding circuit. Then we decode the state and perform a quantum state tomography to obtain the complete five-qubit density matrix. We simulate the error correction operation with the obtained density matrix assuming single-shot measurements and feedforward operations are realized. The results for the magic state are presented in Fig. S10.

TABLE S5. Syndrome table of single-qubit error after decoding.

$Q_5 Q_2 Q_4 Q_3$	Error	Recovery operation
0000	No error	-
0001	X_1	X
1001	X_5	Y
0011	X_2	Y
0111	X_4	-
1100	X_3	-
1010	Y_1	Y
0110	Y_5	Z
1101	Y_2	Z
0101	Y_4	-
0100	Y_3	-
1011	Z_1	Z
1111	Z_5	X
1110	Z_2	X
0010	Z_4	-
1000	Z_3	-

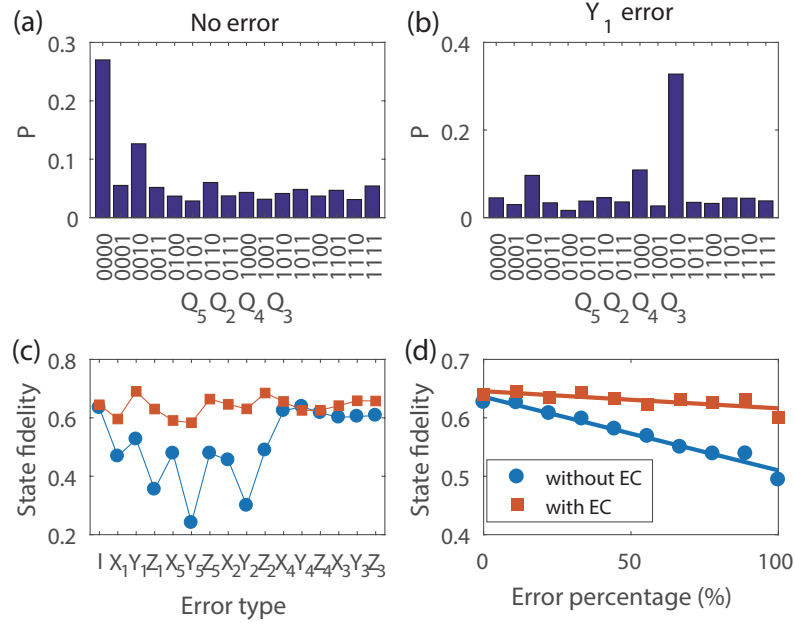


FIG. S10. Verification of error correction after decoding. The projections of the four ancillary qubits on $Z_5 Z_2 Z_4 Z_3$ basis can be used to identify the error type. For an encoded logical $|T\rangle_L$ state, the projections with no error and Y_1 error are presented in (a) and (b), respectively. The single-qubit error is introduced by applying corresponding single-qubit gate on the qubit after encoding process is finished. In (c), the state fidelity after error correction is improved in comparison with no error-correction operation. Similar with Fig. 4(c) in the main text, the result of error correction with different error percentage for logical $|T\rangle_L$ state and single-qubit Y_1 error is presented in (d).

G. Energy relaxation of the logical qubit

To measure the energy relaxation time of the logical qubit, we first prepare the logical state $|0\rangle_L$ and $|1\rangle_L$. Then, after an idling time t_i , we perform a quantum state tomography to obtain the density matrix of the state. We focus on the logical qubit density matrix within the code space. The state fidelity is defined as the trace overlap between the experimentally determined density matrix of the logical state and the ideal state. As shown in Fig. S11, the fidelity decreases over the idling time. Moreover, in comparing with the average energy relaxation time of the five-qubit system, in which the average energy relaxation is determined as the average of the five physical qubit, it is found that the decay rate of the logical state is close to the average energy relaxation in the beginning, and is increasing over time, especially when the idling time is longer than about $1\ \mu\text{s}$. For both $|0\rangle_L$ and $|1\rangle_L$, the fidelity decays to 0.5, indicating the decoherence of logical states into mixed states. Note that the probability of projecting the state to the code space decreases following an exponential decay over time. According to the fitting result, the decay time is about $1.1\ \mu\text{s}$ for $|1\rangle_L$ state and $1.0\ \mu\text{s}$ for $|0\rangle_L$ state.

H. Decoding three qubits

Different from the circuit used in the main text, the decoding process can be equivalently achieved by only applying operations on the top three qubits. This simplification owes to a consequence of locality: no observable on Q_1 can be affected by the omitted independent gate operations of the other qubits. It also highlights the ability of quantum secret sharing with the five-qubit code [10], where after encoding the quantum state into five parties, it can be recovered from operations on the state shared among three parties. As several gates are omitted, the circuit depth is reduced from 122 gates to 93 gates, as shown in Fig. S12(a).

In our experiment, we store the encoded logical state from 0 to 1500 nanoseconds idle time after encoding the single-qubit input state into the logical state. Then we apply the decoding circuit to study the decay of the decoded state fidelity with respect to the idle time.

With input states $|0\rangle$, $|1\rangle$, $|+\rangle$, and $|+i\rangle$, we determine the state fidelity after decoding with zero idle time as 87.4(5)%, 91.6(4)%, 76.7(6)%, and 77.1(6)%, respectively. After quantum process tomography from the four output

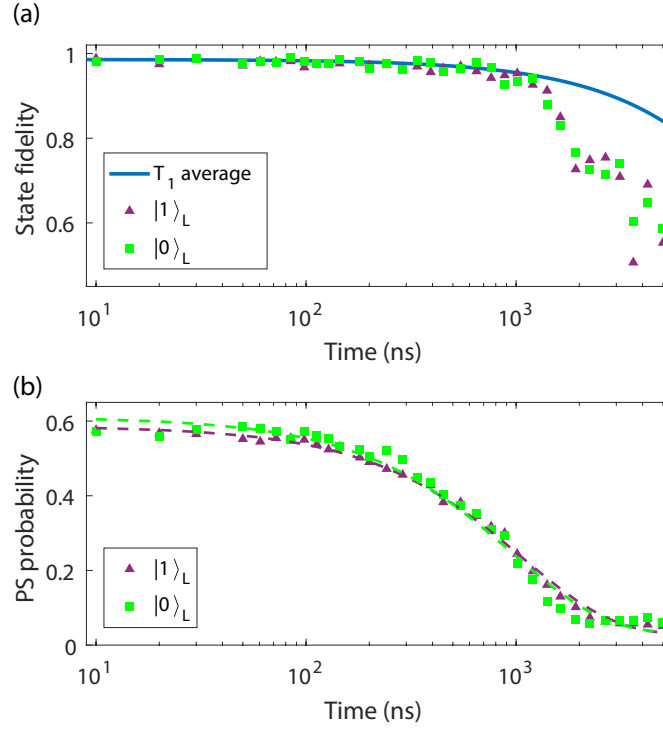


FIG. S11. Energy relaxation of the logical qubit. The prepared logical states are $|1\rangle_L$ (purple triangle), and $|0\rangle_L$ (blue square), respectively. (a) and (b) are the state fidelities to an ideal state with post-processing error decoders and post-selection probabilities, respectively. In (a), the blue solid line corresponds to the theoretical state fidelity with the energy relaxation time being the average of the five physical qubits. The initial theoretical state fidelity is 0.986, which is the average experimental state fidelity of $|0\rangle_L$ and $|1\rangle_L$ with 0 idling time. The post-selection probabilities follow an exponential decay, and the decay time for $|1\rangle_L$, and $|0\rangle_L$, are 1076 ± 90 ns, and 967 ± 137 ns, respectively. The dashed lines in (b) are exponential fittings to data.

states, the process fidelity with zero idle time is determined as 74.5(6)% and it linearly decays with respect to the idle time as shown in Fig. S12(b) and (c).

-
- [1] Gottesman, D. Class of quantum error-correcting codes saturating the quantum hamming bound. *Phys. Rev. A* **54**, 1862–1868 (1996).
 - [2] Barends, R. *et al.* Coherent josephson qubit suitable for scalable quantum integrated circuits. *Physical Review Letters* **111**, 1–6 (2013).
 - [3] Barends, R. *et al.* Superconducting quantum circuits at the surface code threshold for fault tolerance. *Nature* **508**, 500–503 (2014).
 - [4] Kelly, J. *et al.* State preservation by repetitive error detection in a superconducting quantum circuit. *Nature* **519**, 66 (2015).
 - [5] Gong, M. *et al.* Genuine 12-Qubit Entanglement on a Superconducting Quantum Processor. *Physical Review Letters* **122**, 110501 (2019).
 - [6] Martinis, J. M. & Geller, M. R. Fast adiabatic qubit gates using only zz control. *Physical Review A* **90**, 1–9 (2014).
 - [7] Lucero, E. *et al.* Reduced phase error through optimized control of a superconducting qubit. *Physical Review A* **82**, 1–7 (2010).
 - [8] Chuang, I. L. & Nielsen, M. A. Prescription for experimental determination of the dynamics of a quantum black box. *Journal of Modern Optics* **44**, 2455–2467 (1997).
 - [9] Poyatos, J. F., Cirac, J. I. & Zoller, P. Complete characterization of a quantum process: The two-bit quantum gate. *Phys. Rev. Lett.* **78**, 390–393 (1997).
 - [10] Cleve, R., Gottesman, D. & Lo, H.-K. How to share a quantum secret. *Phys. Rev. Lett.* **83**, 648–651 (1999).

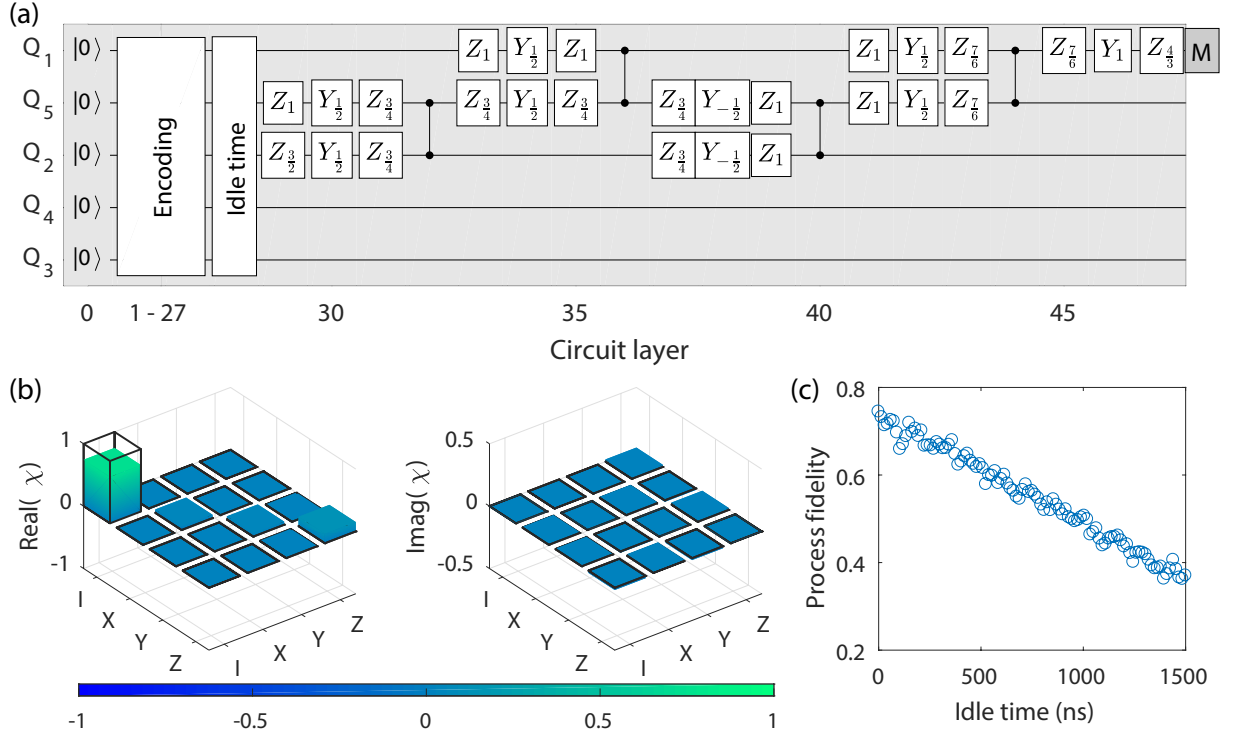


FIG. S12. Decoding of the five-qubit code. (a) Decoding quantum circuit. After the logical state prepared with the encoding circuit, we store the state with 0 to 1500 nano-seconds idle time, and then apply the decoding circuit to map the state back to a single qubit state. The decoding circuit is an inversely ordered encoding circuit, except the gates applied on Q_3 and Q_4 which are omitted because they do not affect the final decoded qubit. Note that the exact hermitian conjugate of the encoding circuit on the first three qubits has minus signs for all the single qubit rotation angles, which, nevertheless is equivalent to the circuit we used in our experiment. (b) The χ_L matrix of the encoding and decoding circuit with 0 idle time. The process fidelity reaches 74.4%. The black-outlined hollow bars correspond to the identical process. (c) The process fidelity of the circuit with respect to the idle time. The fidelity linearly decays with respect to the idle time.